© 2022. Published by The Company of Biologists Ltd | Development (2022) 149, dev200217. doi:10.1242/dev.200217

RESEARCH ARTICLE

The Blimp-1 transcription factor acts in non-neuronal cells to regulate terminal differentiation of the *Drosophila* eye

Hongsu Wang[1], Carolyn A. Morrison[1], Neha Ghosh[1], Joy S. Tea[2,*], Gerald B. Call[2,‡] and Jessica E. Treisman[1,§]

ABSTRACT

The formation of a functional organ such as the eye requires specification of the correct cell types and their terminal differentiation into cells with the appropriate morphologies and functions. Here, we show that the zinc-finger transcription factor Blimp-1 acts in secondary and tertiary pigment cells in the *Drosophila* retina to promote the formation of a bi-convex corneal lens with normal refractive power, and in cone cells to enable complete extension of the photoreceptor rhabdomeres. *Blimp-1* expression depends on the hormone ecdysone, and loss of ecdysone signaling causes similar differentiation defects. Timely termination of *Blimp-1* expression is also important, as its overexpression in the eye has deleterious effects. Our transcriptomic analysis revealed that Blimp-1 regulates the expression of many structural and secreted proteins in the retina. Blimp-1 may function in part by repressing another transcription factor; Slow border cells is highly upregulated in the absence of Blimp-1, and its overexpression reproduces many of the effects of removing *Blimp-1*. This work provides insight into the transcriptional networks and cellular interactions that produce the structures necessary for visual function.

KEY WORDS: Pigment cells, Cone cells, Corneal lens, Blimp-1, Rhabdomeres, *Drosophila*

INTRODUCTION

In organogenesis, terminal differentiation is a vital step during which cell-cell interactions, cellular products and changes in cell morphology all contribute to producing a fully functional organ. Cell differentiation is regulated by transcription factors that are activated in a precise spatial and temporal sequence by extracellular signals, cross-regulatory interactions and epigenetic modifications (Arnes and Sussel, 2015; Gouti et al., 2015). The downstream targets of these transcription factors include proteins that autonomously execute the specialized function of each cell, as well as proteins that establish and maintain the cell-cell interactions that direct the formation of a functionally integrated organ. In general, the transcription factors that initially specify cell fates have been better characterized than those that regulate terminal differentiation.

[1]Skirball Institute for Biomolecular Medicine and Department of Cell Biology, NYU Grossman School of Medicine, 540 First Avenue, New York, NY 10016, USA. [2]Department of Molecular, Cell and Developmental Biology, University of California at Los Angeles, 405 Hilgard Avenue, Los Angeles, CA 90095, USA. *Present address: US Medical Affairs, Genentech, 1 DNA Way, South San Francisco, CA 94080, USA. ‡Present address: Department of Pharmacology, Midwestern University, 19555 N. 59th Ave, Glendale, AZ 85308, USA.

§Author for correspondence (Jessica.Treisman@med.nyu.edu)

C.A.M., 0000-0002-1787-6960; N.G., 0000-0001-6242-4720; J.S.T., 0000-0002-3395-149X; J.E.T., 0000-0002-7453-107X

Handling Editor: Irene Miguel-Aliaga
Received 23 September 2021; Accepted 7 March 2022

The developing *Drosophila* eye is an excellent model system to study cell fate specification and differentiation, as it is a single epithelium in which cell signaling directs equivalent progenitors to produce a well-defined and highly differentiated set of cell types. The compound eye is made of about 800 repetitive units called ommatidia. Each ommatidium is composed of eight photoreceptors, four cone cells and two primary pigment cells, surrounded by a lattice of secondary and tertiary pigment cells and mechanosensory bristles (Fig. 1F). The photoreceptors detect light through their rhabdomeres, stacked membranes packed with rhodopsin that are functionally equivalent to the outer segments of vertebrate rod and cone photoreceptors (Zelhof et al., 2003). Non-neuronal cone cells and primary pigment cells secrete the major components of the corneal lens and the underlying pseudocone; in addition, cone cells are implicated in typical glial support functions such as the control of ion balance, energy resources and sustained neurotransmission (Cagan and Ready, 1989; Charlton-Perkins et al., 2017). Cone cells envelop photoreceptors as they extend their rhabdomeres and contribute to photoreceptor morphogenesis (Charlton-Perkins et al., 2017). As well as producing screening pigments, secondary and tertiary pigment cells are involved in the synthesis and recycling of the chromophore 11-cis-retinal and the neurotransmitter histamine, and secrete some components of the corneal lens (Cagan and Ready, 1989; Chaturvedi et al., 2014; Stahl et al., 2017; Wang et al., 2012).

Specification of the *Drosophila* eye is orchestrated by a set of retinal determination transcription factors, including two homologues of Pax6, which controls eye development throughout the animal kingdom (Glaser et al., 1994; Kumar, 2009; Wawersik and Maas, 2000). These factors activate *glass* (*gl*), which encodes a zinc finger transcription factor that induces photoreceptor differentiation (Bernardo-Garcia et al., 2017; Zelhof et al., 2003). In addition to its effect on photoreceptors, *gl* is cell-autonomously required for the differentiation of the non-neuronal cell types of the eye (Liang et al., 2016; Morrison et al., 2018); therefore, it is not known how each cell type proceeds along a distinct terminal differentiation pathway. Identifying other transcription factors that act combinatorially with Gl would shed light on the cell type-specific regulation of terminal differentiation genes. One candidate for such a factor is Blimp-1, which is predicted to bind to the regulatory regions of many Gl target genes (Morrison et al., 2018). We investigated the possibility that Blimp-1 might control the differentiation of specific retinal cell types.

Blimp-1 is a C2H2 zinc-finger transcription factor that has orthologs in many bilaterians (Bikoff et al., 2009; Nakamura and Extavour, 2016). Human BLIMP1 (also known as PRDM1) regulates the differentiation of various immune cell types, including cytotoxic T cells and antibody-secreting plasma cells (Sciammas and Davis, 2004; Sledzinska et al., 2020), and also specifies primordial germ cells (Fang et al., 2018; Sasaki et al., 2015). *Drosophila* Blimp-1 is known to act in the fat body to regulate the timing of pupation; it is induced by the hormone

Development (2022) 149, dev200217. doi:10.1242/dev.200217

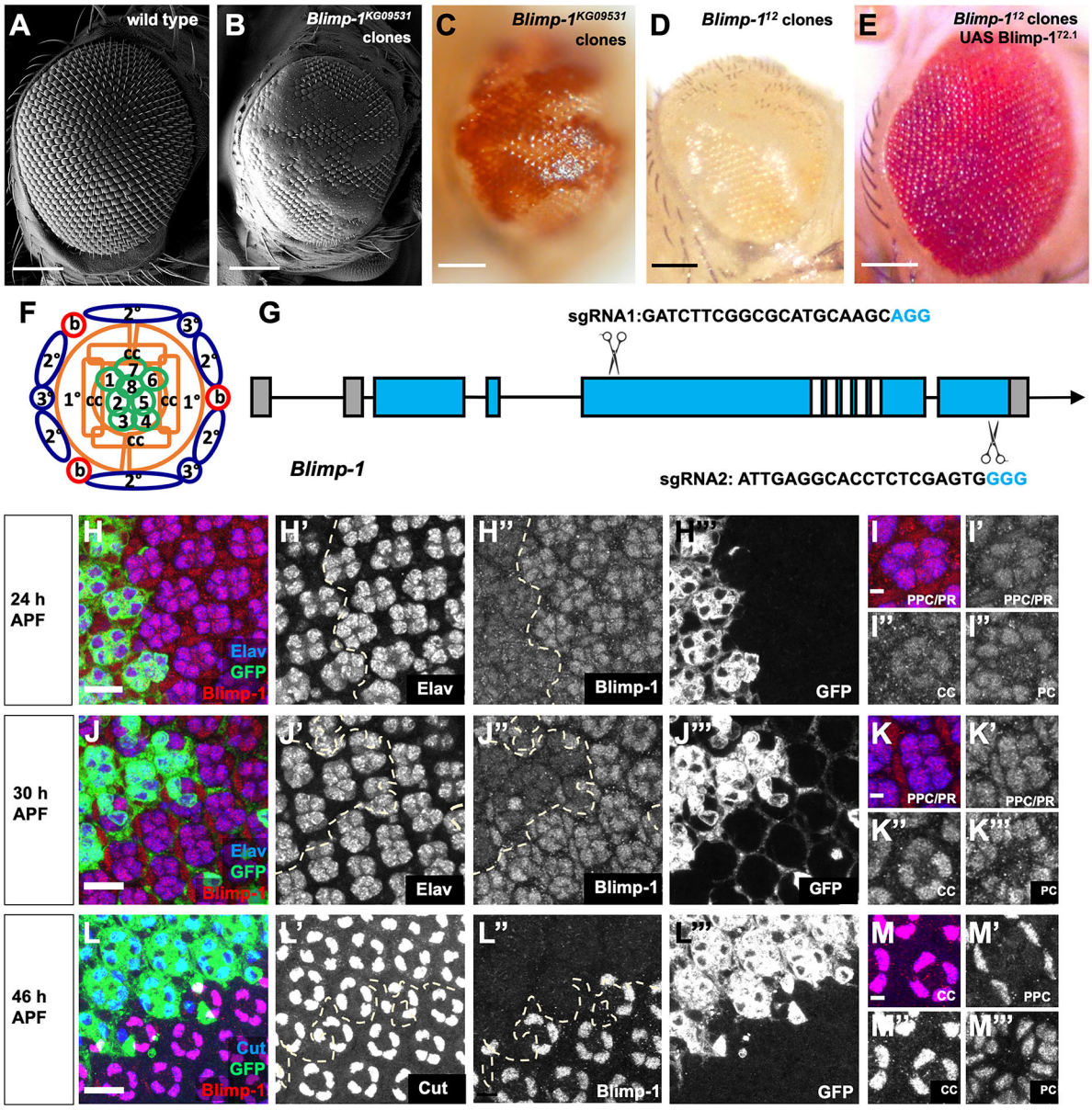

Fig. 1. *Blimp-1* is required for normal eye morphology and is transiently expressed in all retinal cell types. (A,B) Scanning electron micrographs of adult eyes: wild type (A) and *Blimp-1*^{KG09531} homozygous mutant clones (B). The mutant regions are raised and have a smooth surface. (C,D) Adult eyes with *Blimp-1* mutant clones: *Blimp-1*^{KG09531} (mutant regions are darker red; C) and *Blimp-1*^{12} (mutant regions are white; D). (E) Unmarked *Blimp-1*^{12} mutant clones expressing UAS-*Blimp-1*$^{72.1}$. (F) Schematic of an ommatidium in the pupal retina showing the photoreceptors (1-8), cone cells (cc), primary (1°), secondary (2°) and tertiary (3°) pigment cells, and bristles (b). (G) Diagram of the *Blimp-1* RE transcript, showing untranslated regions in gray, coding regions in blue and the five zinc fingers in white. CRISPR mutants *Blimp-1*^{12} and *Blimp-1*^{17} were created by using the two sgRNAs shown to delete the majority of the coding region including the zinc fingers. (H-M) Blimp-1 antibody staining (H″,J″,L″, red in H,J,L) in retinas containing *Blimp-1*^{17} clones positively labeled with GFP (H‴,J‴,L‴, green in H,J,L) and outlined with dashed lines. Photoreceptors are labeled with anti-Elav staining (H′,J′, blue in H,J) in 24 h APF (H,I) and 30 h APF (J,K) retinas. L, M show 46 h APF retinas stained with anti-Cut (L′, blue in L) to mark cone cells. I, K, M show enlargements of single ommatidia from H, J, L, respectively, at planes in which Blimp-1 staining in each of the cell types is visible. M′ shows the plane that contains photoreceptor nuclei, which do not express Blimp-1 at this stage. CC, cone cells; PC, secondary and tertiary pigment cells; PPC, primary pigment cells; PR, photoreceptors. Scale bars: 100 µm (A-E); 10 µm (H,J,L); 2.5 µm (I,K,M).

ecdysone and represses the transcription of *ftz transcription factor 1* (*ftz-f1*), preventing premature pupation (Akagi et al., 2016; Akagi and Ueda, 2011). Blimp-1 is also important for cuticle deposition and tracheal tube maturation in the embryo (Ng et al., 2006; Ozturk-Colak et al., 2016, 2018). The function of Blimp-1 in retinal development has been examined in the mouse, where it is transiently expressed in rod photoreceptors and stabilizes the immature photoreceptor fate by preventing upregulation of bipolar cell-specific genes (Brzezinski et al., 2010, 2013; Wang et al., 2014). The only study of *Drosophila Blimp-1* in the eye showed that RNAi knockdown of *Blimp-1* disrupted corneal lens shape, suggesting that Blimp-1 may regulate corneal lens secretion or morphogenesis (Minami et al., 2016).

In order to investigate how Blimp-1 regulates cell specification and differentiation in the *Drosophila* eye, we characterized the site of *Blimp-1* action by eliminating its function from specific cell types. We found that *Blimp-1* is required in secondary and tertiary pigment cells for the normal bi-convex morphology of the corneal

Development (2022) 149, dev200217. doi:10.1242/dev.200217

lens. We also discovered a separate function for *Blimp-1* in cone cells, where it acts to promote normal photoreceptor morphogenesis, in part by increasing Perlecan levels. We identified potential Blimp-1 target genes by transcriptomic analysis of retinas with loss or gain of *Blimp-1* function. In addition to genes that may directly contribute to corneal lens production and cone cell-photoreceptor interactions, we observed strong upregulation of the transcription factor Slow border cells (Slbo), a C/EBP homologue (Montell et al., 1992), when *Blimp-1* was knocked down, and Slbo overexpression produced a similar phenotype to loss of *Blimp-1*. A subset of the functions of Blimp-1 may be mediated indirectly through repression of *slbo*. Our results show that Blimp-1, which we find to be transiently expressed under the control of the steroid hormone ecdysone, directs the terminal differentiation of the non-neuronal cells of the eye.

RESULTS

Blimp-1 regulates late differentiation of the *Drosophila* eye

The transcriptional networks that control the specification and differentiation of different cell types in the eye are not fully understood. The Gl transcription factor was initially thought to specifically direct photoreceptor differentiation, but was recently shown to also have cell-autonomous functions in cone and pigment cells (Bernardo-Garcia et al., 2017; Liang et al., 2016; Morrison et al., 2018; Moses et al., 1989), implying that other transcription factors must contribute to cell type specificity. We used i-cisTarget (Herrmann et al., 2012; Imrichová et al., 2015) to search for sequence motifs in the regulatory regions of the set of genes that we found to be induced by ectopic expression of Gl (Morrison et al., 2018). One of the most highly enriched motifs matched the binding site for Blimp-1, a PR/SET domain transcription factor related to Gl that contains five zinc fingers (Agawa et al., 2007; Kuo and Calame, 2004; Ng et al., 2006). We therefore chose to investigate the role of Blimp-1 in cell type differentiation in the eye.

In clones of cells homozygous for *Blimp-1*^{KG09531}, a P-element insertion in the first intron, the external surface of the eye became smooth, without clearly demarcated corneal lenses (Fig. 1A-C). To confirm that this phenotype was due to loss of *Blimp-1*, we made *Blimp-1* null mutants (*Blimp-1*^{12} and *Blimp-1*^{17}) by using the CRISPR/Cas9 system to delete the majority of the coding sequence including the zinc fingers (Fig. 1G). Clones homozygous for these deletion mutants also had a smooth external eye surface (Fig. 1D), and this phenotype was rescued by expression of UAS-Blimp-1 (Ozturk-Colak et al., 2016) within the clones (Fig. 1E). A similar phenotype has been reported for *Blimp-1* RNAi expression in the eye (Minami et al., 2016). To determine how loss of *Blimp-1* affects the structure of the eye, we first looked at its expression pattern during the pupal stages using an available antibody (Ng et al., 2006). We stained retinas that contained *Blimp-1* null mutant clones, in order to distinguish true Blimp-1 staining from background cross-reactivity. Blimp-1 was present in all cell types in the retina (schematic in Fig. 1F) from 24 h after puparium formation (APF) to 30 h APF, and was highly expressed in cone and pigment cells at 46 h APF, but lost from photoreceptors at this stage (Fig. 1H-M; Fig. S1B). No expression of Blimp-1 was seen in third instar larval eye discs or 72 h APF pupal retinas (Fig. S1A,C).

In *Blimp-1* mutant clones at mid-pupal stages, we found that photoreceptors labeled with anti-Elav and cone cells labeled with anti-Cut were specified normally (Fig. 1H,J,L). Even in large *Blimp-1* mutant clones generated in a *Minute* (*RpS17*) background (Morata and Ripoll, 1975), patterning of the pigment cell lattice at 42 h APF appeared to be largely normal (Fig. S2B) despite the glossy surface of the adult eye (Fig. S2A). In contrast to its role in the mouse retina, *Blimp-1* thus does not appear to be required for cell fate determination in the *Drosophila* eye.

We next wanted to determine whether Blimp-1 acts downstream of Gl. We observed an increased number of Blimp-1-expressing cells in *gl* mutant clones in the pupal retina (Fig. S3A), suggesting that Gl represses *Blimp-1* expression. The extra Blimp-1-expressing cells did not express the neuronal marker Elav (Fig. S3A) and may be undifferentiated cells. To determine whether misexpression of *Blimp-1* contributes to the *gl* mutant phenotype, we generated *Blimp-1* mutant clones in a *gl* mutant background. However, loss of *Blimp-1* did not improve the patterning defects seen in the *gl* mutant pupal retina (Fig. S3B). If Blimp-1 contributes to the regulation of Gl target genes, its effects may be insufficient to modify the overall *gl* phenotype.

Blimp-1 acts in secondary and tertiary pigment cells to produce a bi-convex corneal lens

In sections through the adult eye, we observed that regions mutant for *Blimp-1* had an altered corneal lens shape (Fig. 2A). Instead of the symmetrical external and internal curvatures seen in wild-type regions (bi-convex lens, Fig. 2B), the external surface was flat (plano-convex lens, Fig. 2C). As Blimp-1 is expressed in multiple cell types, we determined the site at which *Blimp-1* acts to control corneal lens shape by using cell type-specific drivers to express *Blimp-1* RNAi. Because cone cells and primary pigment cells are centrally located (Fig. 2D) and secrete the most abundant corneal lens proteins (Stahl et al., 2017), we expected that loss of *Blimp-1* function from these cells would explain the corneal lens defects. However, corneal lens shape was normal when *Blimp-1* RNAi was expressed in cone and primary pigment cells with *sparkling* (*spa*; also known as *shaven*)-*GAL4* (Jiao et al., 2001) (Fig. S4). In contrast, corneal lens shape was strongly affected when we knocked down *Blimp-1* in secondary and tertiary pigment cells using *54-GAL4* (Lee and Luo, 1999) (Fig. 2E,F). These higher order pigment cells are named for their ability to produce screening pigments; however, they also secrete some components of the corneal lens (Cagan and Ready, 1989; Stahl et al., 2017). In horizontal sections, corneal lenses in whole eyes or in clonal regions that expressed *Blimp-1* RNAi in pigment cells had a plano-convex shape (Fig. 2F,G). Overall, the flat appearance of each individual corneal lens gave the RNAi-expressing regions a smooth and shiny appearance (Fig. 2H). One possible explanation for the raised appearance of these facets could be deposition of excess chitin above the secondary and tertiary pigment cells. However, when we examined eyes that expressed *Blimp-1* RNAi in pigment cells by electron microscopy, we did not observe extra corneal lens material in this position (Fig. 2I,J).

The outer curvature of the corneal lens (air-facing) accounts for most of its refractive power (Stavenga, 2003). To assess the curvature of the outer surface, we measured the outer angle between adjacent corneal lenses (Fig. 2K). Corneal lenses within *Blimp-1*^{17} mutant clones showed a significant increase in this angle to 182±10° (mean±s.d.), compared with the average angle for control clones of 134±6° (Fig. 2L). We also modeled control and *Blimp-1* mutant corneal lenses as thick optic lenses and calculated their focal lengths based on previous studies (Stavenga, 2003) (Fig. 2M,N), with the assumption that the refractive indices of the corneal lens and pseudocone remain the same as measured for wild-type flies (Stavenga, 2003). The radius of the outer surface of the *Blimp-1* mutant corneal lens was treated as infinite. We calculated an average focal length for control corneal lenses of 25.7±1.8 µm, consistent

Development (2022) 149, dev200217. doi:10.1242/dev.200217

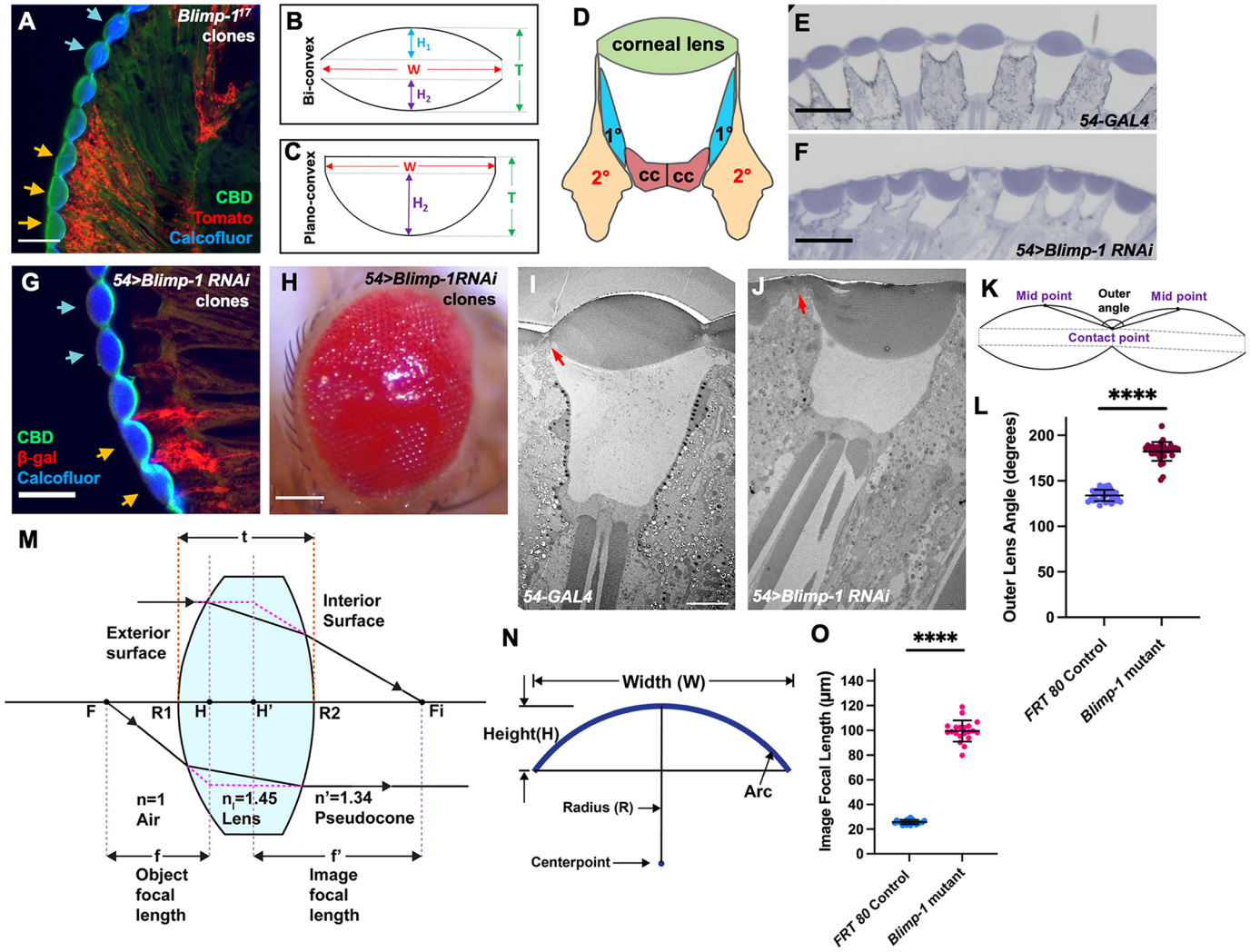

Fig. 2. *Blimp-1* acts in the higher order pigment cells to maintain bi-convex corneal lens morphology. (A) Horizontal section of adult head with *Blimp-1*^{17} clones positively labeled with myristoylated Tomato (red). Corneal lenses are stained with an Alexa488-labeled chitin binding domain (CBD, green) and Calcofluor White (blue); in wild-type regions they have a bi-convex shape (blue arrows), whereas in mutant regions they have a plano-convex shape (yellow arrows). (B) Schematic of the normal bi-convex shape of the *Drosophila* corneal lens in horizontal section. (C) Schematic of the plano-convex lens shape seen in *Blimp-1* mutants. W, width; H_1, height of external corneal lens; H_2, height of internal corneal lens; T, thickness. (D) Schematic of the apical region of an adult ommatidium, showing the positions of cone and primary pigment cells under the central corneal lens and secondary pigment cells at the periphery. (E,F) Plastic sections of adult eyes: control (E) and *Blimp-1* RNAi driven in secondary and tertiary pigment cells by *54-GAL4* (F). (G,H) Adult eyes with clones in which *Blimp-1* RNAi is driven with *54-GAL4*. G shows a horizontal section in which β-gal (red) marks a clone expressing *Blimp-1* RNAi with *54-GAL4*, stained with CBD (green) and Calcofluor White (blue) to detect chitin. Yellow arrows indicate plano-convex and blue arrows bi-convex lenses. H shows an external eye with a smooth surface in the clones. (I,J) Transmission electron micrographs of ommatidia from a control eye (I) and an eye in which *Blimp-1* RNAi is driven with *54-GAL4* (J). Little corneal lens material is deposited above the secondary pigment cells in either case (red arrows). (K) Illustration defining the outer angle of the corneal lens. (L) Quantification of the outer angle of corneal lenses in *Blimp-1* mutant or wild-type control clones, *n*=35 each. (M) Image focal length f′, the parameter that is relevant to fly vision, is calculated using the equations $P1=(n_l-n)/R1$, $P2=(n'-n_l)/R2$, $P3=(-t/n_l)\times P1\times P2$, $P_l=P1+P2+P3$, $f=n/P_l$, $f'=n'/P_l$. F, object focal point; Fi, image focal point; R1, radius of curvature of the exterior surface facing the air; R2, radius of curvature of the interior surface facing the pseudocone; H and H′, principal points; t, thickness of the lens; f, object focal length; n, refractive index of air; n_l, refractive index of lens; n′, refractive index of pseudocone. Equations and refractive indices are those used for wild-type flies (Stavenga, 2003). R2 is a negative number in a bi-convex lens, and R1 is assumed to be infinite in a plano-convex lens. (N) Diagram showing the radius of curvature of a corneal lens surface, which is calculated using the formula $R=H^2+W^2/8H$. (O) Calculated image focal length of corneal lenses in *Blimp-1* mutant and wild-type control clones, *n*=20 each. Data are mean±s.d. ****P<0.0001 (Welch's two-tailed *t*-test). Scale bars: 20 µm (A,E,F,G); 100 µm (H); 10 µm (I, also applies to J).

with the previously reported wild-type value of 26.8±2.3 µm (Stavenga, 2003) (Fig. 2O). The focal length for mutant lenses was increased almost fourfold to 99.4±8.6 µm (Fig. 2O), which is longer than the entire depth of the retina of the mosaic flies, measured at its longest point at the anterior of the eye (90±2.7 µm, *n*=10). In conclusion, the plano-convex corneal lenses formed in *Blimp-1* mutant regions have a dramatically increased image focal length that we predict would make it impossible for them to form a clear image on the retina.

Blimp-1 acts in cone cells to promote normal photoreceptor morphogenesis

We next examined how loss of *Blimp-1* affects photoreceptor development. In clones that were homozygous for *Blimp-1* or in

Development (2022) 149, dev200217. doi:10.1242/dev.200217

eyes in which *Blimp-1* RNAi was expressed in all cell types with the *lGMR-GAL4* driver, photoreceptor rhabdomeres visualized by staining for the leucine-rich repeat protein Chaoptin (Chp) (Krantz and Zipursky, 1990) or the channel Transient receptor potential-like (TrpL) (Niemeyer et al., 1996) were short and disorganized, and photoreceptor nuclei labeled with Elav (Koushika et al., 1996) were mislocalized (Fig. 3A; Fig. S5A). This does not appear to be due to an autonomous requirement for *Blimp-1* in photoreceptors, as expressing *Blimp-1* RNAi specifically in photoreceptors with *elav-GAL4* produced no obvious phenotype (Fig. S6A,B). In contrast, driving *Blimp-1* RNAi with *prospero* (*pros*^{PSG})*-GAL4* (Charlton-Perkins et al., 2017) or *spa-GAL4*, which overlap in cone cells, resulted in similar defects in rhabdomere extension and nuclear arrangement (Fig. 3B,C; Fig. S5B). These defects were autonomous to regions in which *Blimp-1* was lost from cone cells (Fig. 3D). Photoreceptor nuclei, most likely the R8 nuclei that are normally located at the proximal side of the retina, appeared to be displaced to the ends of rhabdomeres, which did not extend as far basally as in wild-type ommatidia (Fig. 3A,C,D,F,G).

Cone cells envelop photoreceptors as they extend their rhabdomeres, and could contribute to photoreceptor morphogenesis

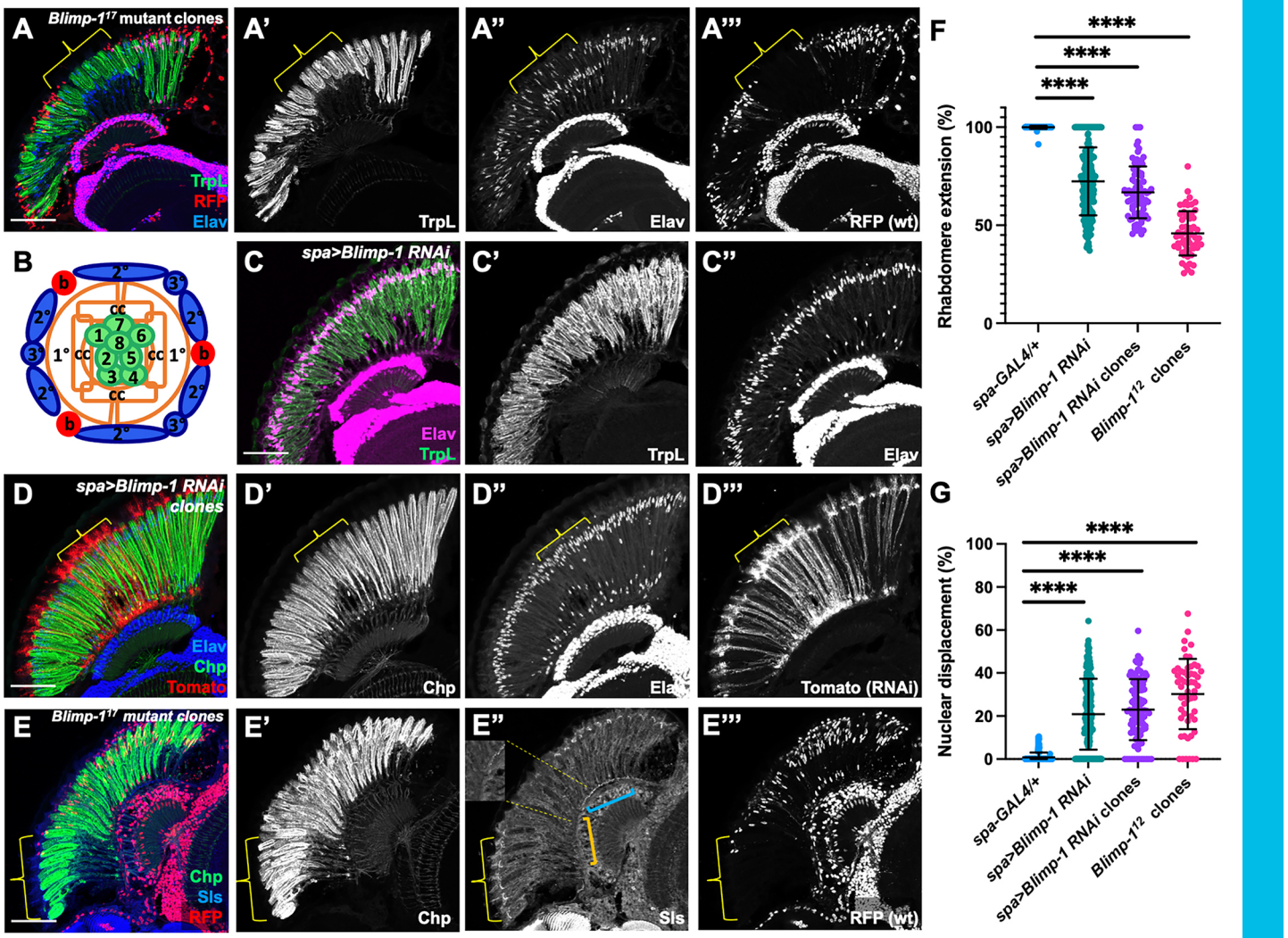

Fig. 3. *Blimp-1* acts in cone cells to generate normal photoreceptor morphology. (A) Horizontal section of adult head in which *Blimp-1*^{17} mutant clones are negatively marked by the absence of nuclear RFP (A‴, red in A). TrpL staining (A′, green in A) marks photoreceptor rhabdomeres and Elav (A″, blue in A) marks neuronal nuclei. Brackets mark clones in which rhabdomeres fail to extend to the proximal side of the retina and photoreceptor nuclei are misplaced. (B) Schematic of an ommatidium representing loss of *Blimp-1* from the cone cells (cc) and primary pigment cells (1°), which express *spa-GAL4*. 1-8, photoreceptors; 2°, secondary pigment cells; 3°, tertiary pigment cells; b, bristles. (C) Horizontal section of adult head in which *Blimp-1* RNAi is driven by *spa-GAL4*. Photoreceptor rhabdomeres marked by TrpL (C′, green in C) fail to extend and nuclei marked by Elav (C″, magenta in C) are disorganized. (D) Horizontal section of adult head containing clones in which *Blimp-1* RNAi and myristoylated Tomato (D‴, red in D) are driven in cone and primary pigment cells with *spa-GAL4*. Chp (D′, green in D) marks photoreceptor rhabdomeres and Elav (D″, blue in D) marks neuronal nuclei. Brackets mark an RNAi clone, which shows a rhabdomere extension defect and disorganized photoreceptor nuclei. (E) Horizontal section of adult head in which *Blimp-1*^{17} mutant clones are negatively marked by the absence of nuclear RFP (E‴, red in E). Chp staining (E′, green in E) marks photoreceptor rhabdomeres and Sls (E″, blue in E) marks cone cell feet. *Blimp-1*^{17} clones show reduced rhabdomere extension and lack Sls staining in the cone cell feet (yellow bracket). Blue bracket indicates wild-type cone cell feet. Inset (E″) shows an enlargement of the indicated region at the border of the clone. (F,G) Quantifications of proximal rhabdomere extension (F) and distal displacement of R8 photoreceptor nuclei (G), defined as a percentage of the length of the retina at that point. Data are mean±s.d. ****P<0.0001 (Welch's two-tailed t-test). n=137 (*spa-GAL4*/+, F), n=231 (*spa>Blimp-1 RNAi*, F), n=86 (*spa>Blimp-1 RNAi* clones, F), n=59 (*Blimp-1*^{12} clones, F), n=210 (*spa-GAL4*/+, G), n=213 (*spa>Blimp-1 RNAi*, G), n=94 (*spa>Blimp-1 RNAi* clones, G) and n=55 (*Blimp-1*^{12} clones, G). Scale bars: 50 µm.

Development (2022) 149, dev200217. doi:10.1242/dev.200217

(Charlton-Perkins et al., 2017). We therefore looked at whether autonomous loss of *Blimp-1* from these cells alters their development. *sallimus* (*sls*) encodes a Titin-like protein that is enriched in cone cell feet (Morrison et al., 2018), which are located at the proximal side of the retina (Cagan and Ready, 1989). We confirmed that Sls colocalized with Fasciclin III in the apical regions of cone cells, and that the staining we observed in cone cell feet was abolished by expressing *sls* RNAi in the retina (Fig. S7). We found that Sls staining was lost from cone cell feet in *Blimp-1* mutant regions, suggesting that cone cell differentiation is disrupted by loss of *Blimp-1* function (Fig. 3E). However, removal of *sls* alone is not sufficient to disrupt photoreceptor rhabdomeres (Fig. S7B). *terribly reduced optic lobes* (*trol*), which encodes the extracellular matrix (ECM) protein Perlecan (Pcan) (Voigt et al., 2002), is another gene that we found to be regulated by Blimp-1 in cone cells (Fig. S8A). Pcan was also localized to cone cell feet (Fig. S8B), and knocking it down in the eye resulted in shortened rhabdomeres (Fig. S8C,D), suggesting that it may contribute to the defective photoreceptor morphogenesis that results from loss of *Blimp-1* in cone cells.

Ecdysone signaling promotes *Blimp-1* expression during development

Blimp-1 expression is known to be regulated by hormonal signaling in both *Drosophila* and mammalian development (Agawa et al., 2007; Ahmed et al., 2016; Akagi et al., 2016; Akagi and Ueda, 2011; Ozturk-Colak et al., 2018). To test whether the hormone ecdysone regulates *Blimp-1* levels in the developing *Drosophila* eye, we reduced ecdysone signaling by knocking down the expression of the ecdysone receptor (EcR). Expressing *EcR* RNAi in all cells in the eye caused phenotypes resembling *Blimp-1* loss-of-function, including a flat external corneal lens surface, shortened photoreceptor rhabdomeres and disordered photoreceptor nuclei (Fig. 4A,B). We next examined Blimp-1 expression in pupal retinas in which clones of cells expressed *EcR* RNAi. Although early expression of Blimp-1 at 30 h APF was only slightly affected in *EcR* RNAi clones (Fig. 4C-E), the stronger expression seen in cone and pigment cells at 41 h APF was dramatically reduced (Fig. 4F-H). These results suggest that upregulation of *Blimp-1* expression in mid-pupal stages by ecdysone signaling is required for normal adult photoreceptor and corneal lens morphology.

Blimp-1 overexpression disrupts photoreceptor and pigment cell morphology

Blimp-1 expression is transient in the eye and was lost from photoreceptors earlier than from the other cell types (Fig. 1J-M). *Blimp-1* mRNA and protein are unstable, enabling it to control the timing of developmental processes (Agawa et al., 2007; Akagi and Ueda, 2011). We tested the effect of Blimp-1 overexpression in the eye by generating clones in which UAS-*Blimp-1* was expressed in all cell types with *lGMR-GAL4* (Fig. S9). In the adult eye, these regions lacked their normal structure and sometimes appeared to be black (Fig. S9B). Sectioning and immunostaining of these eyes revealed defects in both neuronal and non-neuronal cell types. Photoreceptor nuclei misexpressing Blimp-1 were displaced medially (Fig. S9A), the rhabdomeres in each ommatidium had increased levels of Chp and sometimes appeared to be fused together (Fig. S9E,G), and staining for the calcium channel TrpL (Niemeyer et al., 1996) was weaker in some *Blimp-1*-expressing ommatidia (Fig. S9D). Blimp-1 overexpression also affected pigment cell development; Photoreceptor dehydrogenase (Pdh), an enzyme involved in chromophore regeneration that is specific to pigment cells (Wang et al., 2010), showed reduced expression in regions of the adult eye that overexpressed *Blimp-1* (Fig. S9C), and many extra pigment cells remained in the lattice at 42 h APF (Fig. S9F). The arrangement of photoreceptor nuclei was also disrupted when we overexpressed Blimp-1 specifically in photoreceptors, suggesting that extending the period of *Blimp-1* expression in these cells has deleterious effects (Fig. S6C). These results show that timely removal of Blimp-1 is crucial for normal eye development.

Blimp-1 regulates terminal differentiation genes

The corneal lens and photoreceptor defects caused by loss and gain of *Blimp-1* function suggested that terminal differentiation of multiple cell types in the eye was disrupted. To find the target genes of Blimp-1 that could mediate these phenotypes, we carried out a transcriptomic analysis of 48 h APF pupal retinas in which *Blimp-1* was knocked down or overexpressed in all cell types with *lGMR-GAL4*. In retinas expressing *Blimp-1* RNAi, we found 189 genes that were significantly downregulated and 184 genes that were upregulated (Fig. 5A). In retinas overexpressing *Blimp-1*, 514 genes were significantly upregulated and 196 genes downregulated (Fig. 5A). Although some genes were oppositely affected by gain or loss of Blimp-1, as expected for target genes, many of the genes that were induced by Blimp-1 overexpression were not reduced by *Blimp-1* RNAi (Fig. 5B). Some of these genes may not be physiological targets of Blimp-1, and others may not normally be expressed at this developmental stage. The presence of predicted *Blimp-1* binding motifs in the regulatory regions of genes that were upregulated as well as those that were downregulated by loss of *Blimp-1* suggests that Blimp-1 may act as both a transcriptional repressor and an activator (Herrmann et al., 2012; Imrichová et al., 2015) (Table S1; Fig. S10A,B).

Among the genes with known or predicted functions that are regulated by *Blimp-1*, some of the larger classes encode enzymes, cell surface proteins, cuticle proteins and other secreted proteins (Fig. 5C,D; Table S1). *Drosophila* corneal lenses have a cuticular nature, and four major corneal lens proteins have been identified by mass spectrometry. Crystallin and Retinin are secreted from cone and primary pigment cells, whereas Cpr66D and Cpr72Ec are produced by higher order pigment cells (Stahl et al., 2017). The *Blimp-1* corneal lens phenotype is likely to arise from misregulation of proteins secreted by higher order pigment cells, as loss of *Blimp-1* function from cone and primary pigment cells did not affect the corneal lens (Fig. S4). However, *Cpr66D* and *Cpr72Ec* mRNA levels were not significantly altered by *Blimp-1* knockdown. As 79 unique cuticle proteins were found in the adult *Anopheles gambiae* lens using mass spectrometry (Zhou et al., 2016), it is likely that the *Drosophila* corneal lens contains more protein components than have been identified to date. *Blimp-1* loss-of-function may affect uncharacterized corneal lens components that are secreted by the secondary and tertiary pigment cells. The morphology of the corneal lens could also be affected by changes in the proteins that attach it to the pigment cells; for example, Blimp-1 affects the expression of a number of zona pellucida (ZP) domain proteins that have been shown to control the shape of cuticular structures in the late embryo (Fernandes et al., 2010). The photoreceptor phenotypes resulting from *Blimp-1* loss-of-function in the cone cells could potentially reflect changes in the expression of secreted proteins such as Pcan, cytoskeletal proteins such as Sls and cell surface proteins that might promote interactions between photoreceptors and cone cells (Fig. 5C,D). Both *sls* and *trol* were significantly downregulated in retinas expressing *Blimp-1* RNAi (Table S1).

Development (2022) 149, dev200217. doi:10.1242/dev.200217

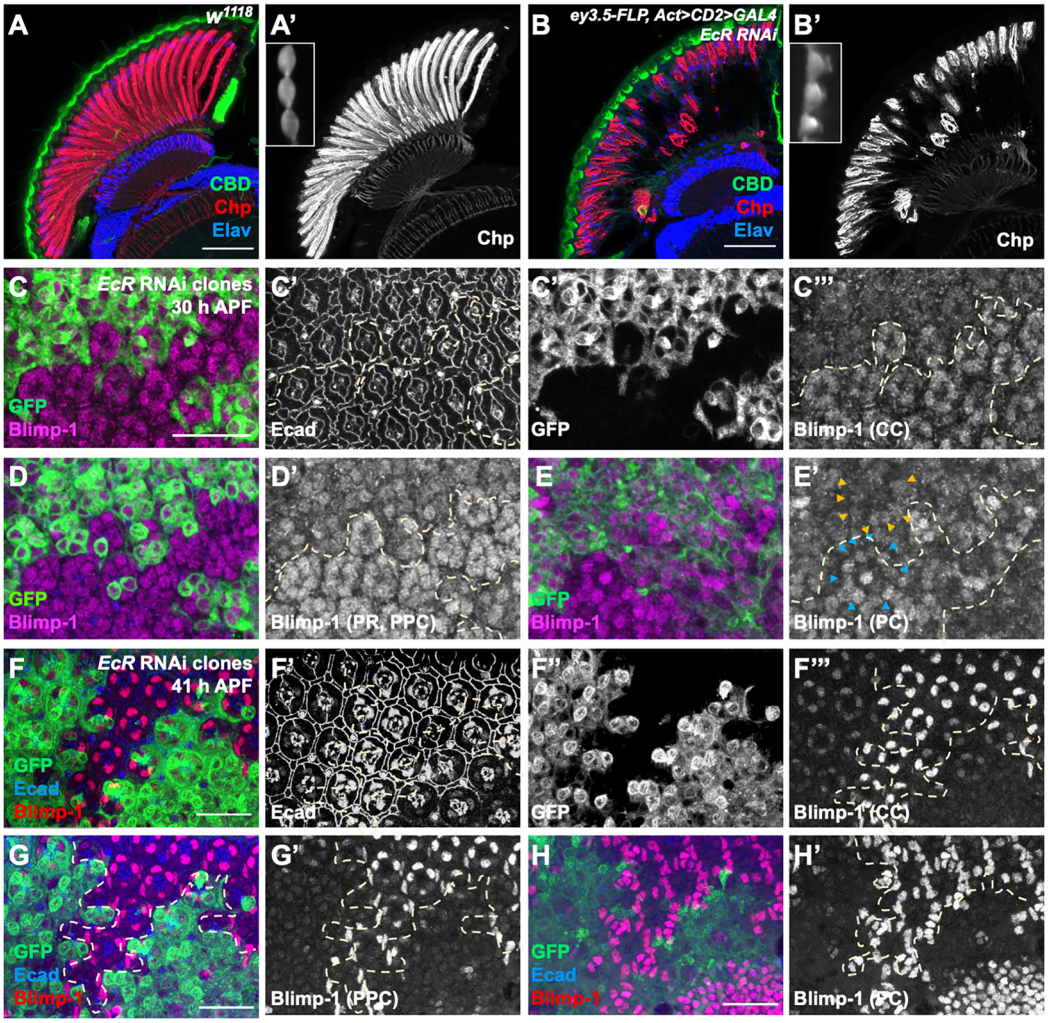

Fig. 4. Ecdysone maintains *Blimp-1* expression in the pupal retina. (A,B) Horizontal sections of adult eyes stained with CBD (green), Elav (blue) and Chp (A′,B′, red in A,B). (A) w^{1118} control. (B) *EcR* RNAi expressed throughout the eye with *ey3.5-FLP*, *Act>CD2>GAL4*. Insets in A′ and B′ show enlargements of corneal lenses from sections stained with Calcofluor White. Loss of EcR results in short rhabdomeres, displaced photoreceptor nuclei and flattened corneal lenses. (C-H) Pupal retinas containing clones expressing *EcR* RNAi with *lGMR*-GAL4, labeled with GFP (C″,F″, green in C-H) and stained for Blimp-1 (C‴,D′,E′, F‴,G′,H′, magenta in C-E, red in F-H) and Ecad to mark apical cell membranes (C′,F′, blue in F-H) at 30 h APF (C-E) and 41 h APF (F-H). Individual panels are confocal sections showing the nuclei of cone cells (C‴,F‴), photoreceptors and primary pigment cells (D′,G′), and higher order pigment cells (E′,H′). Pigment cell nuclei in wild-type (blue) and knockdown (orange) ommatidia are indicated with arrowheads in E′. Blimp-1 levels are slightly reduced in *EcR* RNAi clones (outlined with dashed lines) at 30 h APF and strongly reduced at 46 h APF. Scale bars: 50 µm (A,B); 20 µm (C-H).

Blimp-1 is thought to act downstream of ecdysone to implement temporal regulation of organogenesis as well as the development of the whole organism (Agawa et al., 2007; Akagi et al., 2016; Akagi and Ueda, 2011; Ozturk-Colak et al., 2018). We hypothesized that *Blimp-1* could promote normal eye morphogenesis by ensuring a normal rate of development. We used high-throughput data from modENCODE (Graveley et al., 2011) to determine whether loss of *Blimp-1* function systematically shifted gene expression earlier or later in development. Of the genes with reduced expression in 48 h APF *Blimp-1* RNAi retinas, we found that 59 genes (31%) had their peak expression at 48 h APF, whereas smaller numbers were increasing or decreasing their expression, which is consistent with the notion that Blimp-1 regulates genes with precise developmental timing (Fig. 5E). Among the genes that show increased expression in *Blimp-1* RNAi retinas, we found that almost three times as many were increasing their expression at 48 h APF (40 genes, 21.7%) as were decreasing it at this stage (14 genes, 7.6%) (Fig. 5E). This suggests that loss of *Blimp-1* leads to the premature expression of genes that would normally reach their peak later in development, and that accelerated development may thus contribute to its loss-of-function phenotypes.

Upregulation of *slbo* may contribute to *Blimp-1* loss-of-function phenotypes

The gene that was most highly upregulated in retinas expressing *Blimp-1* RNAi was *slbo* (Fig. 6A), which encodes a transcriptional activator homologous to human CEBPD that contributes to border cell migration in the *Drosophila* ovary (Borghese et al., 2006; Montell et al., 1992). Consistent with the RNA-seq data, we observed *slbo-lacZ* upregulation in $Blimp\text{-}1^{12}$ mutant clones, where it was confined to the non-neuronal cells of the retina (Fig. 6B). Overexpressing *slbo* in otherwise wild-type eyes with *lGMR-GAL4* recapitulated many of the phenotypes of loss-of-*Blimp-1*. The eye assumed a flat and shiny appearance (Fig. 6C-E) with short rhabdomeres and abnormally arranged photoreceptor nuclei

Development (2022) 149, dev200217. doi:10.1242/dev.200217

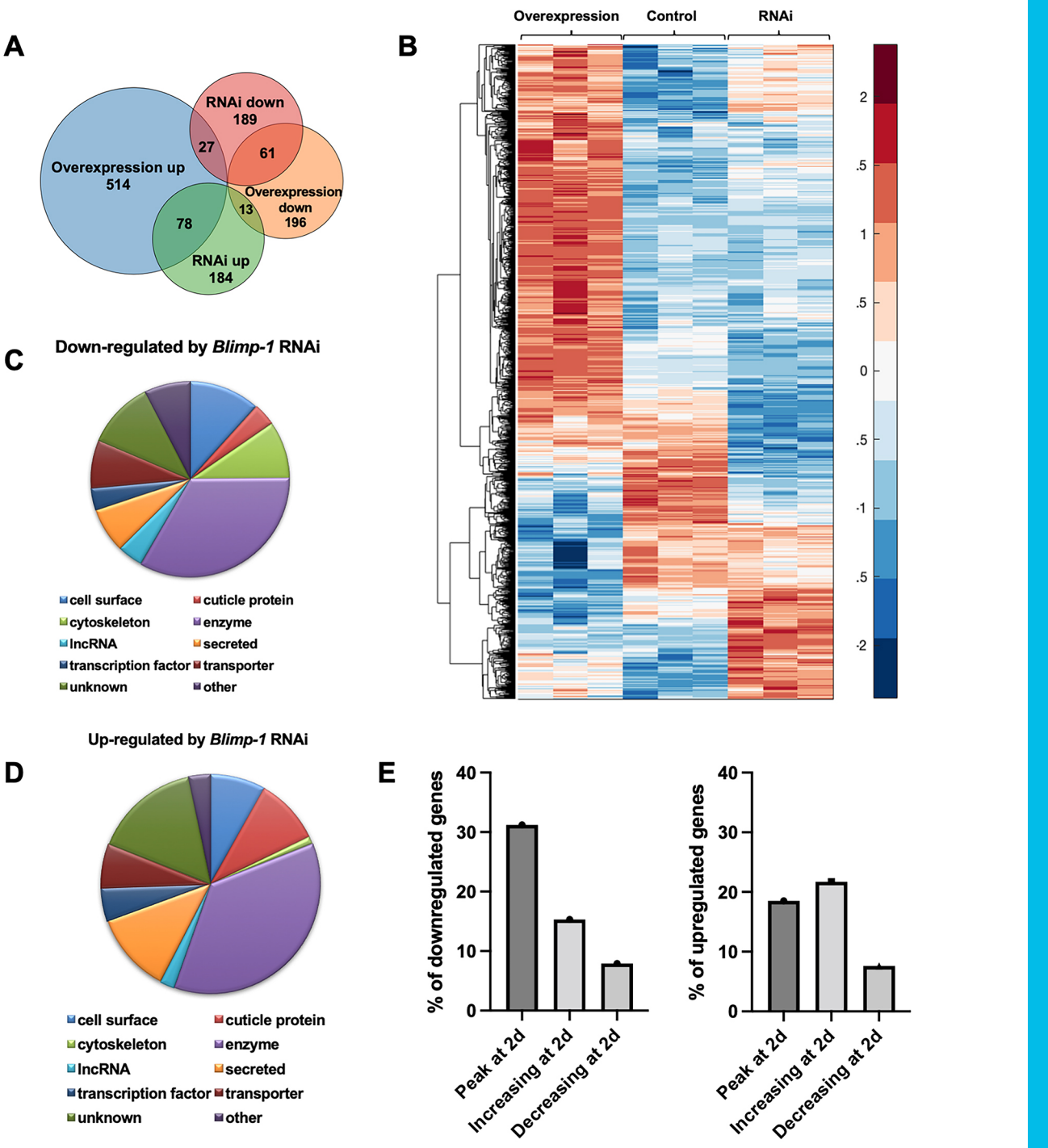

Fig. 5. Blimp-1 regulates genes that may function in terminal differentiation. (A) Euler diagram of the number of genes with significant changes in expression level (log_2 fold change>1, *P*-value>0.05, standard deviation/mean<0.5) induced by *Blimp-1* overexpression or RNAi. (B) Heat map of the expression levels of *Blimp-1*-regulated genes in three conditions: *Blimp-1* overexpression, *IGMR-GAL4*/+ control and *Blimp-1* RNAi. (C,D) Pie charts showing the major categories of genes with reduced (C) or increased (D) expression in retinas expressing *Blimp-1* RNAi. (E) Graphs showing the percentages of genes that are significantly downregulated (left) or upregulated (right) by *Blimp-1* RNAi that have an expression peak at 48 h APF or that are stably increasing or decreasing their expression at this stage.

resembling those caused by *Blimp-1* knockdown (Fig. 6H,I). Overexpression of *slbo* specifically in higher order pigment cells with *54-GAL4* was sufficient to make the corneal lenses become plano-convex (Fig. 6F,G). The similarity between the phenotypes caused by Slbo overexpression and *Blimp-1* loss-of-function suggests that Blimp-1 could regulate the differentiation of cone and pigment cells in part by repressing *slbo*. Consistent with this model, i-cisTarget (Herrmann et al., 2012; Imrichová et al., 2015) predicted Slbo binding sites in a large subset of the genes that showed altered expression after *Blimp-1* knockdown (Fig. S10A,B). However, expressing *Blimp-1* RNAi in *slbo* mutant clones did not visibly rescue its corneal lens and photoreceptor phenotypes (Fig. S10C-F), indicating that loss of *Blimp-1* has significant effects that are independent of *slbo* upregulation.

Development (2022) 149, dev200217. doi:10.1242/dev.200217

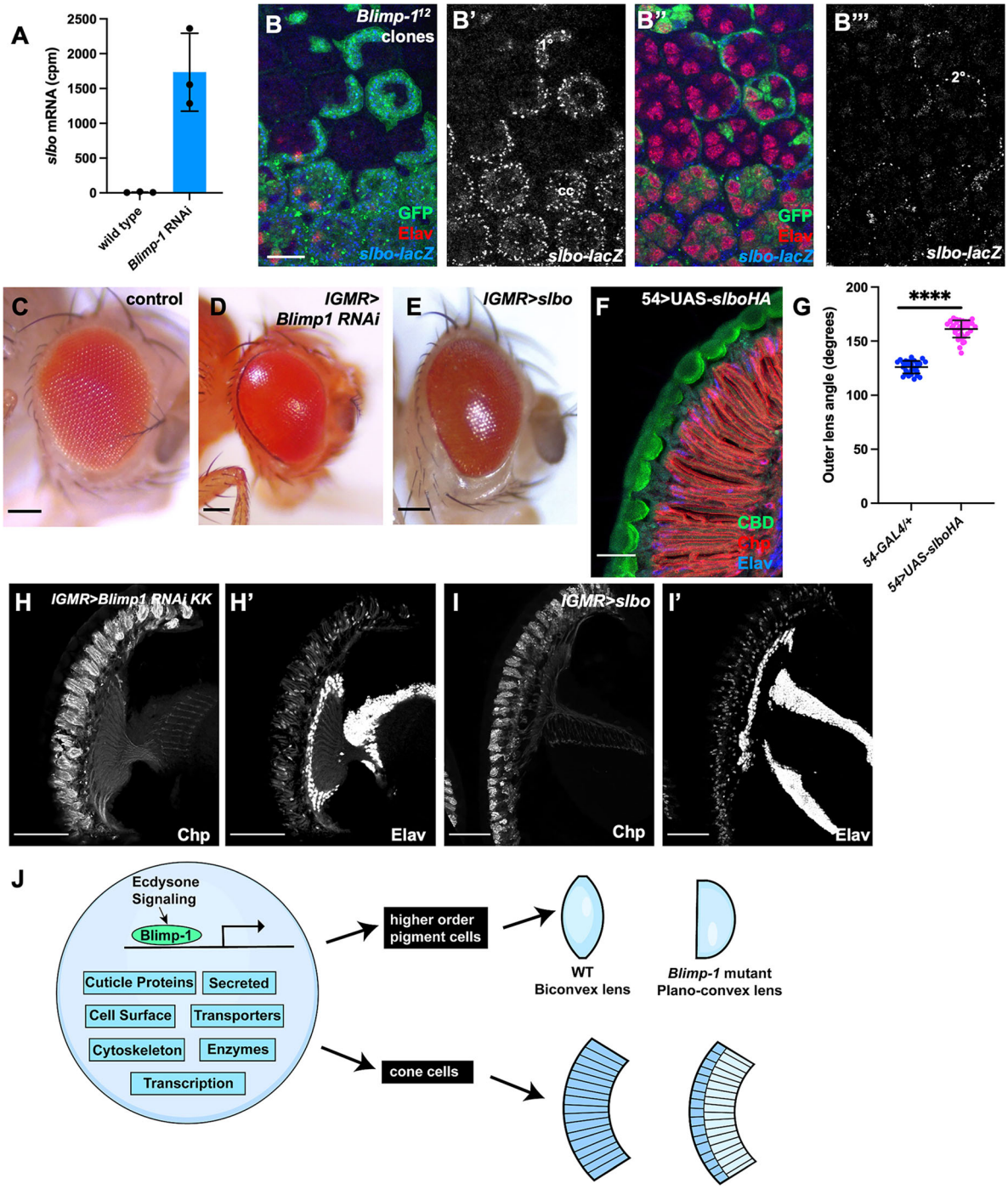

Fig. 6. Slbo overexpression causes phenotypes similar to loss of *Blimp-1*. (A) Graph showing significant upregulation of *slbo* in RNA-seq data from retinas expressing *Blimp-1* RNAi. (B) Confocal sections from a 42 h APF pupal retina in which *Blimp-1* mutant clones are marked with GFP (green), stained with anti-β-galactosidase to reveal *slbo-lacZ* expression (B′,B‴, blue in B,B″) in mutant cone and primary pigment cells (apical section in B,B′) and secondary pigment cells (more basal section in B″,B‴) but not in photoreceptors stained with anti-Elav (red in B,B″). (C-E) Adult eyes: wild type (C), *IGMR-GAL4* driving *Blimp-1* RNAi (D) and *IGMR-GAL4* driving UAS-*slbo* (E). Both *Blimp-1* loss-of-function and *slbo* overexpression cause a similar glossy eye phenotype. (F) Horizontal section of adult eye expressing UAS-*SlboHA* with *54-GAL4* in higher order pigment cells, stained with CBD (green), Chp (red) and Elav (blue) shows plano-convex lenses. (G) Quantification of outer lens angles for *54-GAL4*/+ control and *54-GAL4;* UAS-*SlboHA*, showing mean±s.d. *n*=31 (*54-GAL4*/+) or 36 (*54>SlboHA*). ****P<0.0001 (Welch's two-tailed *t*-test). (H,I) Sections of adult eyes stained for Chp (H,I) and Elav (H′,I′). *IGMR-GAL4* driving *Blimp-1* RNAi (H), *IGMR-GAL4* driving UAS-*slbo* (I). Both manipulations caused shortened rhabdomeres and disorganized photoreceptor nuclei. (J) Model of the Blimp-1 transcriptional network and its major morphological contributions to eye development. Scale bars: 10 µm (B); 100 µm (C-E); 20 µm (F); 50 µm (H-I′).

DISCUSSION

The Blimp-1 transcription factor has been shown to play important regulatory roles in the development of many cell types and organs in both flies and mammals (Agawa et al., 2007; Akagi et al., 2016; Brzezinski et al., 2010; Fu et al., 2017; Lin et al., 2014; Ozturk-Colak et al., 2016, 2018; Sciammas and Davis, 2004; Sledzinska

Development (2022) 149, dev200217. doi:10.1242/dev.200217

et al., 2020). The only reported function for Blimp-1 in the mouse retina is to stabilize the photoreceptor cell fate (Brzezinski et al., 2010, 2013); however, we found that *Drosophila* Blimp-1 acts at a later stage of retinal development to promote the terminal differentiation of several cell types. It has no visible function in photoreceptors, but acts in the cone cells to enable normal photoreceptor rhabdomere extension and in the higher order pigment cells to promote the formation of a biconvex corneal lens (Fig. 6J). Blimp-1 controls the terminal differentiation of these cells by regulating a battery of genes that encode likely structural components of the eye as well as Slbo and other transcription factors. Upregulation of *Blimp-1* expression in the retina requires ecdysone signaling, illustrating a role for steroid hormones in regulating sensory organ morphogenesis.

Blimp-1 acts in non-neuronal cells to regulate corneal lens shape and photoreceptor morphology

Although humans and *Drosophila* have shared common ancestors only in the very distant past and their lenses have distinct molecular compositions, both species evolved bi-convex lens shapes that enable them to focus light effectively onto the retina. The fly corneal lens cannot change its curvature through muscle contractions as the human lens does; to compensate for its fixed parameters, the fly retina is able to detect light throughout its depth (Zhu, 2013). However, the thickness of the retina is insufficient to compensate for the massive reduction in the refractive power of the corneal lens resulting from the plano-convex shape caused by *Blimp-1* loss-of-function, especially as loss of *Blimp-1* also reduces retinal thickness. Loss of curvature on the external surface of *Blimp-1* mutant corneal lenses is more detrimental to their refractive power than flattening of the internal surface facing the pseudocone would be, as the refractive indices of the corneal lens and pseudocone are similar to each other, but quite different from that of air (Stavenga, 2003).

Although major corneal lens proteins such as Crystallin and Retinin are produced by the cone and primary pigment cells (Stahl et al., 2017), *Blimp-1* acts in the more peripheral secondary and tertiary pigment cells to generate the external curvature of the corneal lens. Blimp-1 has been shown to regulate chitin deposition during embryonic cuticle formation and tracheal maturation (Ozturk-Colak et al., 2018), and chitin is a major component of the corneal lens that may determine its shape. Blimp-1 also controls the expression of numerous cuticle proteins that could be secreted from higher-order pigment cells to give the periphery of the corneal lens a composition distinct from the center. Besides regulating the expression of direct structural components of the corneal lens, Blimp-1 could contribute to the bi-convex shape by regulating the forces that pigment cells exert on the periphery of the corneal lens through its effects on the expression of cell surface and cytoskeletal proteins.

In addition to its effect on corneal lens shape, *Blimp-1* loss-of-function causes a defect in photoreceptor morphology. Instead of extending throughout the depth of the retina, rhabdomeres are absent from the proximal retina, where the photoreceptors form stalk-like structures lacking rhabdomere markers. Photoreceptor nuclei are also displaced to the proximal ends of the rhabdomeres. During development, photoreceptors interact with cone cells as they undergo a 90° rotation of their apical membrane surface (Charlton-Perkins and Cook, 2010). Microvilli projecting from this apical membrane subsequently form rhabdomeres that extend proximally down the retina, growing to ∼90 µm in length (Charlton-Perkins and Cook, 2010; Longley and Ready, 1995). As cone cells are known to structurally and physiologically support photoreceptors during development (Charlton-Perkins et al., 2017), loss of *Blimp-1* in these cells may affect their ability to contribute to photoreceptor development. Genes encoding cell surface, cytoskeletal and secreted proteins that we found to be regulated by Blimp-1 (Fig. 5C,D), including *trol*, could promote rhabdomere extension or attachment to an ECM produced by the cone cell feet.

Blimp-1 is necessary to prevent *slbo* expression in the retina

We found that loss of Blimp-1 leads to a dramatic upregulation of the transcription factor Slbo in non-neuronal retinal cells. Overexpressing *slbo* in the eye results in a plano-convex lens and shortened rhabdomeres, similar to what is observed in *Blimp-1* mutants. *slbo* overexpression could thus contribute to the *Blimp-1* loss-of-function phenotypes. However, removing *slbo* is not sufficient to restore normal retinal development in the absence of *Blimp-1*, indicating that at least one crucial target gene requires direct input from Blimp-1 in addition to the absence of Slbo. Two distinct mechanisms, one regulated by Slbo and one by loss of Blimp-1 independently of Slbo, can thus lead to this constellation of phenotypes.

Most previous studies of *slbo* have focused on its requirement for normal border cell migration in the ovary (Montell et al., 1992) and have shown that its overexpression is detrimental to most other tissues (Rorth et al., 2000). As the eye is quite distinct from the ovary in its structure and morphogenesis, it is surprising that only a single transcription factor prevents *slbo* from being expressed there. It is more common to find a factor that is poised for expression when a single repressor is removed in tissues that share a common origin or developmental pathway. For example, *knot* is required for wing patterning but is repressed by Ultrabithorax in the haltere disc, which is a structure homologous to the wing disc (Hersh and Carroll, 2005). It is not known what activators drive *slbo* expression in the absence of repression by Blimp-1. In the ovary, *slbo* is activated by JAK/STAT signaling, which acts early in eye development to promote growth of the larval eye disc, but is not known to function in the pupal retina (Silver and Montell, 2001; Zeidler et al., 1999). The mouse *slbo* homologue *Cebpa* is activated by Blimp-1 in uterine tissues (Goolam et al., 2020), suggesting possible conservation of the regulation of C/EBP genes by Blimp-1, but not of the direction of this effect.

Given the presence of Blimp-1 at the periphery of the developing mouse cornea (Parfitt et al., 2015), our results raise the intriguing possibility that its role in regulating the curvature of refractive surfaces is conserved. Further investigation of this hypothesis may provide insight into the genesis of the refractive disorders that afflict a growing number of people.

MATERIALS AND METHODS

Drosophila genetics

The *Blimp-1* sgRNA sequences GATCTTCGGCGCATGCAAGC (*Blimp-1* sgRNA 1) and ATTGAGGCACCTCTCGAGTG (*Blimp-1* sgRNA 2), identified on www.flyrnai.org/crispr2/, were cloned into pCFD5 (Port and Bullock, 2016) by PCR and Gibson assembly, and the construct was integrated into the attP40 site at 25C6. UAS-*Blimp-1*$^{FLAG\text{-}HA}$ (*Drosophila* Genomics Resource Center clone UFO06327) was integrated into the VK22 site at 57F5. Injections and screening of transgenic flies were carried out by Genetivision. The sgRNA-expressing flies were crossed to *nos-Cas9* [Bloomington *Drosophila* Stock Center (BDSC), #54591] and the progeny were screened for failure to complement the lethality of *Blimp-1*^{KG09531} (BDSC, #15195). PCR analysis showed that two lines that failed to complement (*Blimp-1*^{12} and *Blimp-1*^{17}) carried a 2 kb deletion between the two sgRNA sites.

Development (2022) 149, dev200217. doi:10.1242/dev.200217

Drosophila melanogaster stocks used to generate *Blimp-1* mutant clones were: (1) *UAS-CD8-GFP, ey3.5-FLP; lGMR-GAL4; FRT80, tub-GAL80/TM6B*; (2) *ey-FLP; FRT80, Ubi-His2AvRFP /TM6B*; (3) *ey-FLP; FRT80, RpS17, Ubi-GFP*; (4) *FRT80*, *Blimp-1^{17}/TM6B*; (5) *ey-FLP*; *FRT80, Blimp1^{KG09531}/TM6B*; (6) *slbo-lacZ*; *FRT80*, *Blimp-1^{12}/SM6-TM6B*. Stocks used to generate *Blimp-1* knockdown clones were: (1) *UAS-CD8-GFP, ey3.5-FLP; 54-GAL4, UAS-lacZ; FRT82, tub-GAL80/SM6-TM8B*; (2) *ey-FLP*, *spa-GAL4; UAS-myr-Tomato*; *FRT82*, *tub-GAL80*; (3) *UAS-CD8-GFP, ey3.5-FLP; lGMR-GAL4; FRT82, tub-GAL80/SM6-TM6B*; (4) *UAS-CD8-GFP, ey3.5-FLP; elav-GAL4; FRT82, tub-GAL80/SM6-TM6B*; (5) *UAS-Blimp-1 RNAi BL; FRT82.* Stocks used to generate *Blimp-1* overexpression clones were: (1) *UAS-CD8-GFP, ey3.5-FLP; lGMR-GAL4; FRT82, tub-GAL80*; (2) *UAS-Blimp-1$^{72.1}$; FRT82/SM6-TM6B*; (3) *UAS-Blimp-1$^{FLAG-HA}$; FRT82/SM6-TM6B*. Other stocks used were *54-GAL4, UAS-lacZ/SM6-TM6B* (Lee and Luo, 1999); *spa-GAL4* (Jiao et al., 2001); *lGMR-GAL4* (Wernet et al., 2003); *ey3.5-FLP*, *Act>CD2>GAL4* (BDSC, #35542 and #4780); *pros^{PCG}-GAL4* (Charlton-Perkins et al., 2017); *UAS-Blimp-1 RNAi BL* (HMC04792, BDSC, #57479); *UAS-Blimp-1 RNAi KK* [P{KK107466}VIE-260B, Vienna *Drosophila* Resource Center (VDRC), #108374]; *UAS-slbo* (Rorth et al., 1998); *UAS-slboHA* (FlyORF F000038); *slbo^{8ex22}* (Rorth and Montell, 1992); *gl^{60j}* (Moses et al., 1989); *Blimp-1-GFP.FPTB* (BDSC, #67656); *UAS-Blimp-1$^{72.1}$* (Ozturk-Colak et al., 2016); *UAS-sls RNAi* (TRiP.JF01099); and *UAS-trol RNAi* (P{KK105502}VIE-260B, VDRC, #110494). Stocks used for rescue were: (1) *UAS-CD8-GFP, ey3.5-FLP; lGMR-GAL4; FRT80, tub-GAL80/TM6B*; (2) *UAS-Blimp-1$^{72.1}$; Blimp-1^{12}/SM6-TM6B*. Genotypes used for RNA-seq were: (1) *lGMR-GAL4/UAS-Blimp-1$^{72.1}$*; (2) *lGMR-GAL4/UAS-Blimp-1* RNAi BL; (3) *lGMR-GAL4/+*. Male and female flies were used interchangeably, as no sex-specific differences were observed.

Immunohistochemistry

Pupal retinas were fixed and stained as previously described (Tea et al., 2014). Retina-brain complexes were dissected out of pupae aged from the white prepupal stage and collected in ice-cold PBS in a glass plate. These were fixed for 30 min in 4% formaldehyde in PBS, washed in ice-cold PBS/0.2% Triton X-100 (PBT) for 15 min and incubated overnight at 4°C in primary antibodies in 10% donkey serum in PBT, followed by three 20 min washes in PBT, a 2 h incubation at 4°C in secondary antibodies in PBT and another three 20 min washes in PBT. Retinas were separated from the brain on glass slides and mounted in 80% glycerol in PBS. For cryosectioning, adult heads were fixed for 3-4 h at 4°C in 4% formaldehyde in 0.2 M sodium phosphate buffer (pH 7.2) (PB) after removing the proboscis. Fly heads were glued onto glass rods using nail polish and transferred through a sucrose gradient in PBS consisting of 20 min each in 5%, 10%, 25% and 30% sucrose. Heads were frozen in OCT on dry ice. Then, 12 µm cryosections were cut at −21°C and slides were fixed post-sectioning for 30 min in 0.5% formaldehyde in PB at room temperature. After three 10 min washes in PBT, slides were blocked for 1 h and incubated in primary antibodies overnight at 4°C in 1% bovine serum albumin (BSA) in PBT. After three 20 min washes in PBT, slides were incubated in secondary antibodies in 1% BSA in PBT for 2 h at 4°C and mounted in Fluoromount (Southern Biotech). A 1:5 dilution of Calcofluor White solution (25% in water; Sigma Aldrich, 910090) was included with the secondary antibodies where indicated. The primary antibodies used were: mouse anti-Chp [1:50; Developmental Studies Hybridoma Bank (DSHB), 24B10], chicken anti-GFP (1:400; Invitrogen, A10262), rat anti-Elav (1:100; DSHB, Rat-Elav-7E8A10 anti-elav), mouse anti-Cut (1:10; DSHB, 2B10), rat anti-Ecad (1:10, DSHB, DCAD2), mouse anti-FasIII (1:10, DSHB, 7G10 anti-Fasciclin III), mouse anti-Pros [1:10, DSHB, Prospero (MR1A)], rabbit anti-β-galactosidase (1:5000; MP Biomedicals, 55976), rat anti-Kettin/Sls (1:200; Abcam, ab50585), rabbit anti-DsRed (1:500, Takara Bio, 632496), rabbit anti-TrpL (1:200; Niemeyer et al., 1996), rabbit anti-Pdh (1:200; Wang et al., 2010) and guinea pig anti-Blimp-1 (1:400; Ng et al., 2006). All antibodies were validated either using mutant or knockdown conditions as shown, or by verifying that the staining pattern matched previously published descriptions. The secondary antibodies used were from either Jackson ImmunoResearch (Cy3 or Cy5 conjugates used at 1:200) or Invitrogen (Alexa488 conjugates used at 1:1000). Images were acquired on a Leica SP8 confocal microscope and processed using ImageJ and Adobe Photoshop. Outer lens angles were measured with ImageJ according to the diagram in Fig. 2K, and rhabdomere length and nuclear position were normalized to the depth of the retina measured using ImageJ. Significance was calculated using Welch's two-tailed *t*-tests. Sample sizes for quantifications were not predefined and no samples were excluded.

Chitin binding probe preparation

The plasmid pYZ205 (New England Biolabs), which encodes a 6XHis-SNAP-chitin binding domain (CBD) fusion construct, was transformed into *Escherichia coli BL21DE3* and protein expression was induced with 1 mM IPTG at OD_{600} of 0.6 at 37°C for 4 h in Luria Broth with 50 mg/ml ampicillin. The protein was isolated using nickel-NTA agarose resin and eluted in 1 ml fractions with elution buffer [50 mM NaH_2PO_4 (pH 7.2), 300 mM NaCl, 250 mM imidazole, 1 mM DTT]. The eluted proteins were quantified on a Nanodrop Spectrophotometer and their purity was checked by SDS-PAGE. The protein fractions with the highest purity and quantity were selected and dialyzed in phosphate buffer [50 mM NaH_2PO_4 (pH 7.2), 100 mM NaCl, 1 mM DTT] overnight at 4°C. Dialyzed SNAP-CBD protein was adjusted to a final concentration of 5 µM in phosphate buffer and incubated with 10 µM SNAP substrate fluorophore (SNAP-surface Alexa Fluor 488, New England Biolabs, #S9129 or SNAP-surface Alexa Fluor 546, New England Biolabs, #S9132) at 37°C for 1 h. The fluorescently labeled probes were dialyzed in phosphate buffer overnight at 4°C to remove unreacted substrates and stored in 50% glycerol at −20°C. SNAP-CBD-probes were used at a final dilution of 1:200 in immunohistochemistry experiments.

Plastic sections and electron microscopy

Adult heads were cut in half and fixed in freshly made fixative containing 2.5% glutaraldehyde, 2% paraformaldehyde and 0.05% Triton X-100 in 0.1 M sodium cacodylate buffer (pH 7.2) on a rotator for at least 4 h until all heads had sunk to the bottom of the tube, and then in the same fixative without Triton X-100 overnight at 4°C on a rotator. After washing in PBS, the heads were post-fixed in 1% OsO_4 in PBS for 1.5 h, dehydrated in an ethanol series (30%, 50%, 70%, 85%, 95%, 100%), rinsed twice with propylene oxide and embedded in EMbed812 epoxy resin (Electron Microscopy Sciences). Then 500 nm semi-thin horizontal sections were mounted on a glass slide and baked on a hot plate overnight at 60°C. The sections were stained with 0.1% Toluidine Blue, dried on a hot plate and cover-slipped with Permount™ mounting medium (Electron Microscopy Sciences). Images were taken on a Zeiss Axioplan microscope and processed in Adobe Photoshop. For transmission electron microscopy, 70 nm ultra-thin sections were cut and mounted on formvar-coated slot grids and stained with uranyl acetate and lead citrate (Hess et al., 2006). Electron microscopy imaging was performed on a Talos120C transmission electron microscope (Thermo Fisher Scientific) and recorded using a Gatan (4k×4k) OneView Camera with Digital Micrograph software (Gatan).

For scanning electron microscopy, flies were adhered to tape on microscope slides with nail polish and the eye images were initially captured as light micrographs (Nikon E600 equipped with a Nikon Coolpix 4500 camera) and subsequently as natural scanning electron micrographs (Hitachi 2460N Scanning Electron Microscope, 180×).

RNA isolation and RNA-seq

Pupal retinas (with attached lamina and medulla) were dissected from triplicate samples of 30 animals of each genotype and RNA was extracted using Trizol (Invitrogen). RNA quality and quantity was assessed using the Bio-analyzer 2100 (Agilent). Library preparation and sequencing was carried out by the NYU Genome Technology Center. Libraries were constructed using Illumina TruSeq Stranded mRNA (#20020595), with 250 ng of total RNA as input, and 10 cycles of PCR amplification. Samples were sequenced using single lane Hiseq 4000, paired end read 50. RNA-seq data were analyzed using the sns/rna-star pipeline (https://igordot.github.io/sns/routes/rna-star.html) and the differential expression analyses were carried out using the sns/rna-star-groups-dge pipeline (https://igordot.github.io/sns/routes/rna-star-groups-dge.html). Sequencing reads were mapped to the reference genome (dm6) using the STAR aligner (v2.6.1d)

(Dobin et al., 2013). Alignments were guided by a Gene Transfer Format (GTF) file. The mean read insert sizes and their standard deviations were calculated using Picard tools (v.2.18.20) (http://broadinstitute.github.io/picard). The read count tables were generated using subread (v1.6.3) (Liao et al., 2014), normalized based on their library size factors using DEseq2 (Love et al., 2014), and differential expression analysis was performed. To compare the level of similarity among the samples and their replicates, we used principal component analysis. Genes were considered significantly changed and were included in the heat map if the $\log_2$ fold change for either overexpression or knockdown was >1, P<0.05, and standard deviation/mean of the three replicates was <0.5. The heat map was constructed in Matlab R2017a (https://www.mathworks.com) and the Euler diagram was made using Biovinci software (Bioturing).

Acknowledgements
We thank Sofia Araujo, Leonard Dobens, Craig Montell, the Bloomington *Drosophila* Stock Center, the Vienna *Drosophila* RNAi Center, the *Drosophila* Genomics Resource Center and the Developmental Studies Hybridoma Bank for fly stocks and reagents. Essential information for this study was provided by Flybase. We thank NYULH DART Microscopy Laboratory members Alice Liang, Chris Petzold, Kristen Dancel Manning and Joseph Sall for consultation and assistance with plastic sections and electron microscopy, and this core is partially funded by NYU Cancer Center Support Grant NIH/NCI P30CA016087. We are grateful to Yutong Zhang, Shaowen Jiang and Alireza Khodadadi-Jamayran for assistance with the RNA-seq experiment and analysis. We thank DanQing He and Ariel Hairston for technical assistance. The manuscript was improved by the critical comments of Jane Hubbard and Maria Bustillo. We thank Utpal Banerjee, UCLA (funded by a Howard Hughes Medical Institute Professors Grant) for support during the collection of some of the data.

Competing interests
The authors declare no competing or financial interests.

Author contributions
Conceptualization: H.W., C.A.M., N.G., G.C., J.E.T.; Investigation: H.W., C.A.M., N.G., J.S.T., G.C., J.E.T.; Data curation: H.W.; Writing - original draft: H.W.; Writing - review & editing: C.A.M., N.G., G.C., J.E.T.; Supervision: J.E.T.; Funding acquisition: J.E.T.

Funding
This work was funded by the National Institutes of Health (R01 EY013777 and R21 EY031442 to J.E.T.). Deposited in PMC for release after 12 months.

Data availability
RNA-seq data are available from NCBI GEO under accession number GSE183734.

Peer review history
The peer review history is available online at https://journals.biologists.com/dev/article-lookup/doi/10.1242/dev.200217.

References
Agawa, Y., Sarhan, M., Kageyama, Y., Akagi, K., Takai, M., Hashiyama, K., Wada, T., Handa, H., Iwamatsu, A., Hirose, S. et al. (2007). *Drosophila* Blimp-1 is a transient transcriptional repressor that controls timing of the ecdysone-induced developmental pathway. *Mol. Cell. Biol.* **27**, 8739-8747. doi:10.1128/MCB.01304-07

Ahmed, M. I., Elias, S., Mould, A. W., Bikoff, E. K. and Robertson, E. J. (2016). The transcriptional repressor Blimp1 is expressed in rare luminal progenitors and is essential for mammary gland development. *Development* **143**, 1663-1673. doi:10.1242/dev.136358

Akagi, K. and Ueda, H. (2011). Regulatory mechanisms of ecdysone-inducible Blimp-1 encoding a transcriptional repressor that is important for the prepupal development in *Drosophila*. *Dev. Growth Differ.* **53**, 697-703. doi:10.1111/j.1440-169X.2011.01276.x

Akagi, K., Sarhan, M., Sultan, A.-R. S., Nishida, H., Koie, A., Nakayama, T. and Ueda, H. (2016). A biological timer in the fat body comprising Blimp-1, betaFtz-f1 and Shade regulates pupation timing in *Drosophila melanogaster*. *Development* **143**, 2410-2416. doi:10.1242/dev.133595

Arnes, L. and Sussel, L. (2015). Epigenetic modifications and long noncoding RNAs influence pancreas development and function. *Trends Genet.* **31**, 290-299. doi:10.1016/j.tig.2015.02.008

Bernardo-Garcia, F. J., Humberg, T.-H., Fritsch, C. and Sprecher, S. G. (2017). Successive requirement of Glass and Hazy for photoreceptor specification and maintenance in *Drosophila*. *Fly* **11**, 112-120. doi:10.1080/19336934.2016.1244591

Bikoff, E. K., Morgan, M. A. and Robertson, E. J. (2009). An expanding job description for Blimp-1/PRDM1. *Curr. Opin. Genet. Dev.* **19**, 379-385. doi:10.1016/j.gde.2009.05.005

Borghese, L., Fletcher, G., Mathieu, J., Atzberger, A., Eades, W. C., Cagan, R. L. and Rørth, P. (2006). Systematic analysis of the transcriptional switch inducing migration of border cells. *Dev. Cell* **10**, 497-508. doi:10.1016/j.devcel.2006.02.004

Brzezinski, J. A. T., Lamba, D. A. and Reh, T. A. (2010). Blimp1 controls photoreceptor versus bipolar cell fate choice during retinal development. *Development* **137**, 619-629. doi:10.1242/dev.043968

Brzezinski, J. A. T., Uoon Park, K. and Reh, T. A. (2013). Blimp1 (Prdm1) prevents re-specification of photoreceptors into retinal bipolar cells by restricting competence. *Dev. Biol.* **384**, 194-204. doi:10.1016/j.ydbio.2013.10.006

Cagan, R. L. and Ready, D. F. (1989). The emergence of order in the *Drosophila* pupal retina. *Dev. Biol.* **136**, 346-362. doi:10.1016/0012-1606(89)90261-3

Charlton-Perkins, M. and Cook, T. A. (2010). Building a fly eye: terminal differentiation events of the retina, corneal lens, and pigmented epithelia. *Curr. Top. Dev. Biol.* **93**, 129-173. doi:10.1016/B978-0-12-385044-7.00005-9

Charlton-Perkins, M. A., Sendler, E. D., Buschbeck, E. K. and Cook, T. A. (2017). Multifunctional glial support by Semper cells in the *Drosophila* retina. *PLoS Genet.* **13**, e1006782. doi:10.1371/journal.pgen.1006782

Chaturvedi, R., Reddig, K. and Li, H.-S. (2014). Long-distance mechanism of neurotransmitter recycling mediated by glial network facilitates visual function in *Drosophila*. *Proc. Natl. Acad. Sci. USA* **111**, 2812-2817. doi:10.1073/pnas.1323714111

Dobin, A., Davis, C. A., Schlesinger, F., Drenkow, J., Zaleski, C., Jha, S., Batut, P., Chaisson, M. and Gingeras, T. R. (2013). STAR: ultrafast universal RNA-seq aligner. *Bioinformatics* **29**, 15-21. doi:10.1093/bioinformatics/bts635

Fang, F., Angulo, B., Xia, N., Sukhwani, M., Wang, Z., Carey, C. C., Mazurie, A., Cui, J., Wilkinson, R., Wiedenheft, B. et al. (2018). A PAX5-OCT4-PRDM1 developmental switch specifies human primordial germ cells. *Nat. Cell Biol.* **20**, 655-665. doi:10.1038/s41556-018-0094-3

Fernandes, I., Chanut-Delalande, H., Ferrer, P., Latapie, Y., Waltzer, L., Affolter, M., Payre, F. and Plaza, S. (2010). Zona pellucida domain proteins remodel the apical compartment for localized cell shape changes. *Dev. Cell* **18**, 64-76. doi:10.1016/j.devcel.2009.11.009

Fu, S.-H., Yeh, L.-T., Chu, C.-C., Yen, B. L.-J. and Sytwu, H.-K. (2017). New insights into Blimp-1 in T lymphocytes: a divergent regulator of cell destiny and effector function. *J. Biomed. Sci.* **24**, 49. doi:10.1186/s12929-017-0354-8

Glaser, T., Jepeal, L., Edwards, J. G., Young, S. R., Favor, J. and Maas, R. L. (1994). *PAX6* gene dosage effect in a family with congenital cataracts, aniridia, anophthalmia and central nervous system defects. *Nat. Genet.* **7**, 463-471. doi:10.1038/ng0894-463

Goolam, M., Xypolita, M.-E., Costello, I., Lydon, J. P., DeMayo, F. J., Bikoff, E. K., Robertson, E. J. and Mould, A. W. (2020). The transcriptional repressor Blimp1/PRDM1 regulates the maternal decidual response in mice. *Nat. Commun.* **11**, 2782. doi:10.1038/s41467-020-16603-z

Gouti, M., Metzis, V. and Briscoe, J. (2015). The route to spinal cord cell types: a tale of signals and switches. *Trends Genet.* **31**, 282-289. doi:10.1016/j.tig.2015.03.001

Graveley, B. R., Brooks, A. N., Carlson, J. W., Duff, M. O., Landolin, J. M., Yang, L., Artieri, C. G., van Baren, M. J., Boley, N., Booth, B. W. et al. (2011). The developmental transcriptome of *Drosophila melanogaster*. *Nature* **471**, 473-479. doi:10.1038/nature09715

Herrmann, C., Van de Sande, B., Potier, D. and Aerts, S. (2012). i-cisTarget: an integrative genomics method for the prediction of regulatory features and cis-regulatory modules. *Nucleic Acids Res.* **40**, e114. doi:10.1093/nar/gks543

Hersh, B. M. and Carroll, S. B. (2005). Direct regulation of *knot* gene expression by Ultrabithorax and the evolution of cis-regulatory elements in *Drosophila*. *Development* **132**, 1567-1577. doi:10.1242/dev.01737

Hess, M. W., Pfaller, K., Hampölz, B., Longato, S., Teis, D., Flörl, A., Gutleben, K. and Huber, L. A. (2006). Microscopy of the *Drosophila* facet eye: vademecum for standardized fixation, embedding, and sectioning. *Microsc. Res. Tech.* **69**, 93-98. doi:10.1002/jemt.20268

Imrichová, H., Hulselmans, G., Atak, Z. K., Potier, D. and Aerts, S. (2015). i-cisTarget 2015 update: generalized cis-regulatory enrichment analysis in human, mouse and fly. *Nucleic Acids Res.* **43**, W57-W64. doi:10.1093/nar/gkv395

Jiao, R., Daube, M., Duan, H., Zou, Y., Frei, E. and Noll, M. (2001). Headless flies generated by developmental pathway interference. *Development* **128**, 3307-3319. doi:10.1242/dev.128.17.3307

Koushika, S. P., Lisbin, M. J. and White, K. (1996). ELAV, a *Drosophila* neuron-specific protein, mediates the generation of an alternatively spliced neural protein isoform. *Curr. Biol.* **6**, 1634-1641. doi:10.1016/S0960-9822(02)70787-2

Krantz, D. E. and Zipursky, S. L. (1990). *Drosophila* Chaoptin, a member of the leucine-rich repeat family, is a photoreceptor cell-specific adhesion molecule. *EMBO J.* **9**, 1969-1977. doi:10.1002/j.1460-2075.1990.tb08325.x

Kumar, J. P. (2009). The molecular circuitry governing retinal determination. *Biochim. Biophys. Acta* **1789**, 306-314. doi:10.1016/j.bbagrm.2008.10.001

Kuo, T. C. and Calame, K. L. (2004). B lymphocyte-induced maturation protein (Blimp)-1, IFN regulatory factor (IRF)-1, and IRF-2 can bind to the same regulatory sites. *J. Immunol.* **173**, 5556-5563. doi:10.4049/jimmunol.173.9.5556

Lee, T. and Luo, L. (1999). Mosaic analysis with a repressible cell marker for studies of gene function in neuronal morphogenesis. *Neuron* **22**, 451-461. doi:10.1016/S0896-6273(00)80701-1

Liang, X., Mahato, S., Hemmerich, C. and Zelhof, A. C. (2016). Two temporal functions of Glass: Ommatidium patterning and photoreceptor differentiation. *Dev. Biol.* **414**, 4-20. doi:10.1016/j.ydbio.2016.04.012

Liao, Y., Smyth, G. K. and Shi, W. (2014). featureCounts: an efficient general purpose program for assigning sequence reads to genomic features. *Bioinformatics* **30**, 923-930. doi:10.1093/bioinformatics/btt656

Lin, I.-Y., Chiu, F.-L., Yeang, C.-H., Chen, H.-F., Chuang, C.-Y., Yang, S.-Y., Hou, P.-S., Sintupisut, N., Ho, H.-N., Kuo, H.-C. et al. (2014). Suppression of the *SOX2* neural effector gene by PRDM1 promotes human germ cell fate in embryonic stem cells. *Stem Cell Rep.* **2**, 189-204. doi:10.1016/j.stemcr.2013.12.009

Longley, R. L., Jr and Ready, D. F. (1995). Integrins and the development of three-dimensional structure in the *Drosophila* compound eye. *Dev. Biol.* **171**, 415-433. doi:10.1006/dbio.1995.1292

Love, M. I., Huber, W. and Anders, S. (2014). Moderated estimation of fold change and dispersion for RNA-seq data with DESeq2. *Genome Biol.* **15**, 550. doi:10.1186/s13059-014-0550-8

Minami, R., Sato, C., Yamahama, Y., Kubo, H., Hariyama, T. and Kimura, K.-I. (2016). An RNAi screen for genes involved in nanoscale protrusion formation on corneal lens in *Drosophila melanogaster*. *Zoolog. Sci.* **33**, 583-591. doi:10.2108/zs160105

Montell, D. J., Rorth, P. and Spradling, A. C. (1992). *slow border cells*, a locus required for a developmentally regulated cell migration during oogenesis, encodes *Drosophila* C/EBP. *Cell* **71**, 51-62. doi:10.1016/0092-8674(92)90265-E

Morata, G. and Ripoll, P. (1975). *Minutes*: mutants of *Drosophila* autonomously affecting cell division rate. *Dev. Biol.* **42**, 211-221. doi:10.1016/0012-1606(75)90330-9

Morrison, C. A., Chen, H., Cook, T., Brown, S. and Treisman, J. E. (2018). Glass promotes the differentiation of neuronal and non-neuronal cell types in the *Drosophila* eye. *PLoS Genet.* **14**, e1007173. doi:10.1371/journal.pgen.1007173

Moses, K., Ellis, M. C. and Rubin, G. M. (1989). The *glass* gene encodes a zinc-finger protein required by *Drosophila* photoreceptor cells. *Nature* **340**, 531-536. doi:10.1038/340531a0

Nakamura, T. and Extavour, C. G. (2016). The transcriptional repressor Blimp-1 acts downstream of BMP signaling to generate primordial germ cells in the cricket *Gryllus bimaculatus*. *Development* **143**, 255-263. doi:10.1242/dev.127563

Ng, T., Yu, F. and Roy, S. (2006). A homologue of the vertebrate SET domain and zinc finger protein Blimp-1 regulates terminal differentiation of the tracheal system in the *Drosophila* embryo. *Dev. Genes Evol.* **216**, 243-252. doi:10.1007/s00427-005-0044-5

Niemeyer, B. A., Suzuki, E., Scott, K., Jalink, K. and Zuker, C. S. (1996). The *Drosophila* light-activated conductance is composed of the two channels TRP and TRPL. *Cell* **85**, 651-659. doi:10.1016/S0092-8674(00)81232-5

Ozturk-Colak, A., Moussian, B., Araujo, S. J. and Casanova, J. (2016). A feedback mechanism converts individual cell features into a supracellular ECM structure in *Drosophila* trachea. *eLife* **5**, e09373. doi:10.7554/eLife.09373

Ozturk-Colak, A., Stephan-Otto Attolini, C., Casanova, J. and Araujo, S. J. (2018). Blimp-1 mediates tracheal lumen maturation in *Drosophila melanogaster*. *Genetics* **210**, 653-663. doi:10.1534/genetics.118.301444

Parfitt, G. J., Kavianpour, B., Wu, K. L., Xie, Y., Brown, D. J. and Jester, J. V. (2015). Immunofluorescence tomography of mouse ocular surface epithelial stem cells and their niche microenvironment. *Invest. Ophthalmol. Vis. Sci.* **56**, 7338-7344. doi:10.1167/iovs.15-18038

Port, F. and Bullock, S. L. (2016). Augmenting CRISPR applications in *Drosophila* with tRNA-flanked sgRNAs. *Nat. Methods* **13**, 852-854. doi:10.1038/nmeth.3972

Rorth, P. and Montell, D. J. (1992). *Drosophila* C/EBP: a tissue-specific DNA-binding protein required for embryonic development. *Genes Dev.* **6**, 2299-2311. doi:10.1101/gad.6.12a.2299

Rorth, P., Szabo, K., Bailey, A., Laverty, T., Rehm, J., Rubin, G. M., Weigmann, K., Milan, M., Benes, V., Ansorge, W. et al. (1998). Systematic gain-of-function genetics in *Drosophila*. *Development* **125**, 1049-1057. doi:10.1242/dev.125.6.1049

Rorth, P., Szabo, K. and Texido, G. (2000). The level of C/EBP protein is critical for cell migration during *Drosophila* oogenesis and is tightly controlled by regulated degradation. *Mol. Cell* **6**, 23-30. doi:10.1016/S1097-2765(05)00008-0

Sasaki, K., Yokobayashi, S., Nakamura, T., Okamoto, I., Yabuta, Y., Kurimoto, K., Ohta, H., Moritoki, Y., Iwatani, C., Tsuchiya, H. et al. (2015). Robust in vitro induction of human germ cell fate from pluripotent stem cells. *Cell Stem Cell* **17**, 178-194. doi:10.1016/j.stem.2015.06.014

Sciammas, R. and Davis, M. M. (2004). Modular nature of Blimp-1 in the regulation of gene expression during B cell maturation. *J. Immunol.* **172**, 5427-5440. doi:10.4049/jimmunol.172.9.5427

Silver, D. L. and Montell, D. J. (2001). Paracrine signaling through the JAK/STAT pathway activates invasive behavior of ovarian epithelial cells in *Drosophila*. *Cell* **107**, 831-841. doi:10.1016/S0092-8674(01)00607-9

Sledzinska, A., Vila de Mucha, M., Bergerhoff, K., Hotblack, A., Demane, D. F., Ghorani, E., Akarca, A. U., Marzolini, M. A. V., Solomon, I., Vargas, F. A. et al. (2020). Regulatory T cells restrain Interleukin-2- and Blimp-1-dependent acquisition of cytotoxic function by CD4(+) T cells. *Immunity* **52**, 151-166.e156. doi:10.1016/j.immuni.2019.12.007

Stahl, A. L., Charlton-Perkins, M., Buschbeck, E. K. and Cook, T. A. (2017). The cuticular nature of corneal lenses in *Drosophila melanogaster*. *Dev. Genes Evol.* **227**, 271-278. doi:10.1007/s00427-017-0582-7

Stavenga, D. G. (2003). Angular and spectral sensitivity of fly photoreceptors. II. Dependence on facet lens F-number and rhabdomere type in *Drosophila*. *J. Comp. Physiol. A Neuroethol. Sens. Neural Behav. Physiol.* **189**, 189-202. doi:10.1007/s00359-003-0390-6

Tea, J. S., Cespedes, A., Dawson, D., Banerjee, U. and Call, G. B. (2014). Dissection and mounting of *Drosophila* pupal eye discs. *J Vis Exp.*, e52315. doi:10.3791/52315

Voigt, A., Pflanz, R., Schäfer, U. and Jäckle, H. (2002). Perlecan participates in proliferation activation of quiescent *Drosophila* neuroblasts. *Dev. Dyn.* **224**, 403-412. doi:10.1002/dvdy.10120

Wang, X., Wang, T., Jiao, Y., von Lintig, J. and Montell, C. (2010). Requirement for an enzymatic visual cycle in *Drosophila*. *Curr. Biol.* **20**, 93-102. doi:10.1016/j.cub.2009.12.022

Wang, X., Wang, T., Ni, J. D., von Lintig, J. and Montell, C. (2012). The *Drosophila* visual cycle and de novo chromophore synthesis depends on *rdhB*. *J. Neurosci.* **32**, 3485-3491. doi:10.1523/JNEUROSCI.5350-11.2012

Wang, S., Sengel, C., Emerson, M. M. and Cepko, C. L. (2014). A gene regulatory network controls the binary fate decision of rod and bipolar cells in the vertebrate retina. *Dev. Cell* **30**, 513-527. doi:10.1016/j.devcel.2014.07.018

Wawersik, S. and Maas, R. L. (2000). Vertebrate eye development as modeled in *Drosophila*. *Hum. Mol. Genet.* **9**, 917-925. doi:10.1093/hmg/9.6.917

Wernet, M. F., Labhart, T., Baumann, F., Mazzoni, E. O., Pichaud, F. and Desplan, C. (2003). Homothorax switches function of *Drosophila* photoreceptors from color to polarized light sensors. *Cell* **115**, 267-279. doi:10.1016/S0092-8674(03)00848-1

Zeidler, M. P., Perrimon, N. and Strutt, D. I. (1999). Polarity determination in the *Drosophila* eye: a novel role for *unpaired* and JAK/STAT signaling. *Genes Dev.* **13**, 1342-1353. doi:10.1101/gad.13.10.1342

Zelhof, A. C., Koundakjian, E., Scully, A. L., Hardy, R. W. and Pounds, L. (2003). Mutation of the photoreceptor specific homeodomain gene *Pph13* results in defects in phototransduction and rhabdomere morphogenesis. *Development* **130**, 4383-4392. doi:10.1242/dev.00651